LA-UR-01-1570
Approved for public release;
distribution is unlimited.

Title: **Multiscale thermal-infrared measurements of the Mauna Loa caldera, Hawaii**

Author(s): Lee Balick, Alan Gillespie, Elsa Abbott, Don Sabol, Anne Kahle, Christoph Borel, and Malcolm Pendergast

Submitted to:

http://lib-www.lanl.gov/la-pubs/00357139.pdf

Multiscale thermal-infrared measurements of the Mauna Loa caldera, Hawaii

Lee Balick[1], Alan Gillespie[2], Elsa Abbott[3],
Don Sabol[2], Anne Kahle[3], Christoph Borel[1], Malcolm Pendergast[4]

1. Los Alamos National Laboratory, Los Alamos, NM
2. University of Washington, Seattle, WA
3. Jet Propulsion Laboratory, Pasadena, CA
4. SMP Enterprises, Martinez GA

ABSTRACT

Until recently, most thermal infrared measurements of natural scenes have been made at disparate scales, typically 10^{-3}-10^{-2} m (spectra) and 10^{2}-10^{3} m (satellite images), with occasional airborne images (10^{1}m) filling the gap. Temperature and emissivity fields are spatially heterogeneous over a similar range of scales, depending on scene composition. A common problem for the land surface, therefore, has been relating field spectral and temperature measurements to satellite data, yet in many cases this is necessary if satellite data are to be interpreted to yield meaningful information about the land surface. Recently, three new satellites with thermal imaging capability at the 10^{1}-10^{2}m scale have been launched: MTI, TERRA, and Landsat 7. MTI acquires multispectral images in the mid-infrared (3-5μm) and longwave infrared (8-10μm) with 20m resolution. ASTER and MODIS aboard TERRA acquire multispectral longwave images at 90m and 500-1000m, respectively, and MODIS also acquires multispectral mid-infrared images. Landsat 7 acquires broadband longwave images at 60m. As part of an experiment to validate the temperature and thermal emissivity values calculated from MTI and ASTER images, we have targeted the summit region of Mauna Loa for field characterization and near-simultaneous satellite imaging, both on daytime and nighttime overpasses, and compare the results to previously acquired 10^{-1}m airborne images, ground-level multispectral FLIR images, and the field spectra. Mauna Loa was chosen in large part because the 4x6km summit caldera, flooded with fresh basalt in 1984, appears to be spectrally homogeneous at scales between 10^{-1} and 10^{2}m, facilitating the comparison of sensed temperature. The validation results suggest that, with careful atmospheric compensation, it is possible to match ground measurements with measurements from space, and to use the Mauna Loa validation site for cross-comparison of thermal infrared sensors and temperature/emissivity extraction algorithms.

Keywords: Temperature, Scale, Mauna Loa, Remote Sensing

INTRODUCTION

1.1 Objectives

With the recent advent of multiband spaceborne thermal infrared sensors with high spectral resolution, it has become desirable to develop standard test areas that can be used to validate and compare radiometric measurements and temperature and emissivity data calculated from them. This seemingly straightforward task requires primarily a multi-pixel homogeneous and unchanging area that can be characterized on the ground and imaged routinely by the spaceborne sensors. Commonly, large areas of water and dry lake beds in deserts have been used for this purpose. Surface radiometry studies indicate that lakes and ocean sites may be used in radiometric calibration. However, for temperature and emissivity separation algorithms sites of low emissivity contrast such as water, and sites with high emissivity contrast such as rock may be treated differently[1]. Therefore, it is necessary to establish validation sites over both rock and water. Furthermore, most playas are unsatisfactory because they are subject to intermittent flooding, following which the surface emissivity changes as the surface desiccates and clay films are eroded. A validation site comprising an unvegetated rock surface is the best candidate.

Furthermore, experience has shown that emissivity retrieval is sensitive to accurate atmospheric compensation[2,3]. Because atmospheric effects are greatest at low elevations, sea-level sites are not well suited for comparing instruments and temperature/emissivity separation algorithms. Comparisons of sensor-derived and field measurements there are

most likely to shed light on the reliability of the atmospheric compensation algorithm, not the temperature and emissivity recovery *per se*. For this purpose, a high-altitude site consisting of ~150,000 m^2 of unvegetated, homogeneous bedrock is necessary. We propose such a site in the summit caldera of the ~4000m-high volcano, Mauna Loa, on the island of Hawai'i (Figure 1). The purpose of this article is to determine if the site is suitably homogeneous that its emissivity at the pixel scale can be characterized by a reasonable number (~10^2) of laboratory or field spectra, all over an area large enough to encompass 20 or more pixels from satellite images, such that it is suitable for validation and cross-calibration of multiband, longwave thermal infrared data.

1.2 Validation site

The 0.4x0.5km validation site consists of flat, unweathered and compositionally homogeneous pahoehoe basalt erupted in 1984 from a central rift or fissure in the summit of Mauna Loa. The lava largely filled the 4x6km^2 summit caldera.

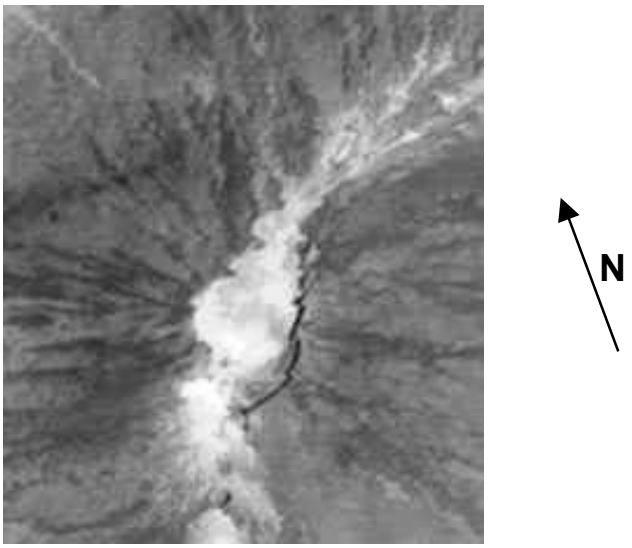

Figure 1. ASTER image of the Mauna Loa summit caldera obtained at 11:21 local time on 14 July, 00.

The validation site is bounded on the southeast by the caldera wall, ~75m high. The northern margin is defined by pumiceous ejecta from the central rift, spectrally distinct from the pahoehoe. The western margin is defined by subtle spectral differences evident in 1985 images taken by the airborne TIMS scanner[4] and more recent MTI data. The lava within the site is broken into ~3m cooling polygons; the glassy crust (<1cm thick) of the pahoehoe has in places spalled, so that the lava surface consists of small loose chips, unmodified glassy pahoehoe, and the more vesicular substrate. In addition, deep cracks between the polygons, which contribute low-contrast cavity (blackbody) radiation, albeit for small areas. Thus, at the local scale of the laboratory spectral measurement (~5cm^2) the emissivity of the lava has the potential to be variable.

There are three important questions in evaluating the spectral homogeneity of the site: 1) are the endmember spectra (glassy crust, substrate) different as viewed by the sensors? 2) what is the spatial scale of variability? and 3) are there any overlooked sources of spectral variability? The first question is readily addressed by spectral measurement of the glassy chips and substrate, but the second question is more difficult to answer. From visual inspection, we know that the scene is variable at the 10^{-2}-10^0 m scale, but we cannot be sure at what scale the mixing fractions of the endmember spectra stabilize, or if they do. The third question is also difficult to address, since we lack an expedient method of identifying samples that we cannot visually discriminate.

2. METHOD

2.1 Data sources

We collected ground samples from the Mauna Loa validation site for laboratory spectral measurement at the Jet Propulsion Laboratory. The spectra were measured using a Nicolet 520 FTIR spectrophotometer at 4 cm-1 spectral resolution from 2.08 to 16 μm. Individual interferograms are obtained with this instrument in slightly less than 1 s and

1000 interferograms were averaged to obtain a good signal-to-noise level. The Nicolet spectrometer measures hemispherical reflectance from samples ~2cm in diameter, and our hemispheric measurements, made using the 20cm integrating sphere, were mathematically converted to emissivity using Kirchhoff's Law. Replicate measurements indicate that the precision of the emissivity spectra is ±0.002, equivalent to the NEΔT of the spaceborne imaging systems (Table 1). The hand samples were collected from a east-west transect from the southeastern rim of the caldera at the eastern most corner of the intensive study area, though the study area, slightly across the central rift, and into the more variable areas of the caldera. At a spacing of about 33m, a cluster of samples was taken within a 2m radius of the central location. A total of 125 emissivity spectra were ultimately measured. The samples in a cluster were chosen to represent the extreme representative lava types at each locality. Fractional amounts of each lava type, estimated visually in percent, were tabulated.

The emissivity measurements were complemented by radiometer measurements made at the times of satellite overpasses. One set was made using hand-held Everest radiometers at a fixed station and roving in the vicinity. Another set was taken with Heimann radiometers in the easternmost corner of the study area within the field of view of a thermal infrared camera on the caldera rim. One unit was stationary, logging data every 10 seconds, while the other was moved within the area automatically logging temperature and GPS coordinates at 10 or 1 second intervals.

Advanced Spaceborne Thermal Emission Radiometer (ASTER) images were acquired from NASA's Terra satellite at 11:21 am (local time) 14 July, 2000. Multispectral Thermal Imager (MTI) data were acquired at 12:49 pm the next day, 15 July 2000. An ASTER image of brightness temperature near the intensive study area is shown in Figure 1 and a similar image from MTI is shown in Figure 2a. The most pertinent features of the satellite sensors are summarized in Table 1**.**

Table 1. Important ASTER and MTI Characteristics

	ASTER	MTI
Number of Thermal IR bands	5	5
Ground sample distance	90m	20m
$NE\Delta T_{300K\ (K)}$	0.2K	0.1K

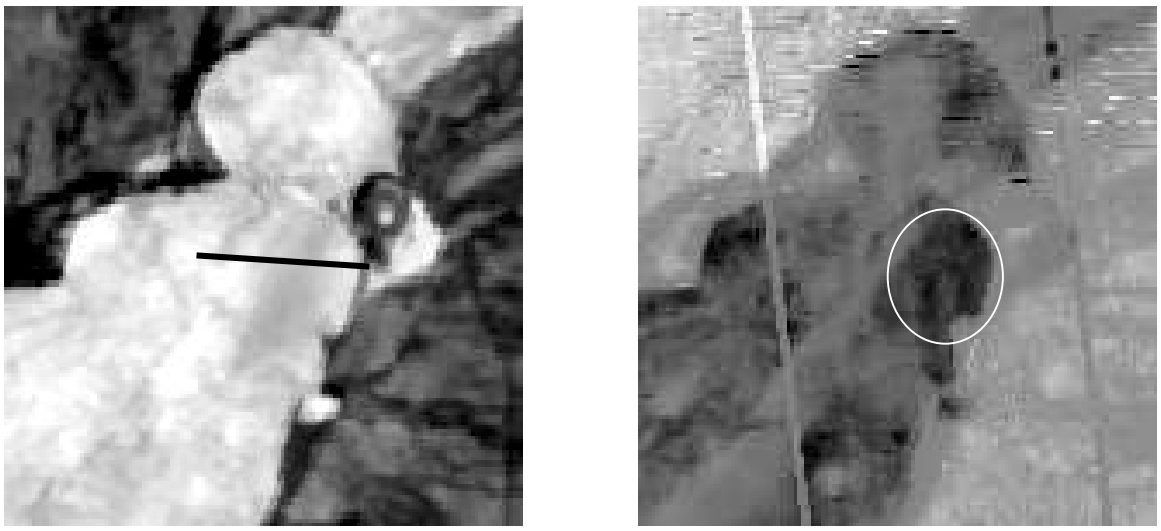

Figure 2. Retrieved physical temperature (a) and emissivity (b) for the MTI image on 15 July, 00. The approximate transect location is shown in (a) and the intensive study area is outlined in (b). The diagonal lines in the emissivity image are due to bad pixels whose effects have since been corrected in MTI imagery

2.2 Analysis

In order to relate the field and satellite data, taken at greatly different scales, the causes of spatial and temporal variation of the radiance measurements must be understood and accounted for in both sampling and analysis. It is desirable to assess the performance of the satellite data and temperature/emissivity recovery algorithms for both

temperature and emissivity. Surface emissivity is the easier parameter to address: the emissivity of rock is constant on the time scale of years, and so once its spatial variability over the validation site is characterized, suitable laboratory or field spectral measurements can be used to validate emissivity images. The effects of emissivity on brightness temperature, in the image and in ground measurements, can also be assessed, statistically.

In addition to emissivity, brightness temperature responds to thermal properties of the lava (density, heat capacity, conductivity) and the history of heating by the sun and cooling radiatively and by wind. It may fluctuate a few degrees on a time scale of minutes. Therefore, field measurements can be used to validate "snapshot" satellite images only over large areas (compared to eddies, for example), because only for such areas is the temperature stable on the short time scale. Its effects on measured radiances can be separated from the effects of temporal variations of temperature. (on the field data - temporal variations may masquerade as spatial variations in a snapshot satellite image. One task, then, is to characterize the spatial variation (uniformity) characteristics of emissivity at various spatial scales so that proper ground sampling and temperature measurements can be made during field campaigns. However, the spatial variation of temperature is subject to significant temporal fluctuations resulting from variations of the energy budget. These fluctuations can be attributed to eddies or wind speed changes which move through a scene and result in spatial variations of temperature if image resolution is nearly the same spatial scale. Therefore, temporal fluctuations must also be taken into account if satellite calibration and algorithm validation is to be precise. Thus the time variation of temperature must be understood.

2.2.1 **Image processing**

Images from both sensors were atmospherically compensated using National Center for Environmental Prediction (NCEP) atmospheric profiles, compiled from available point measurements and reported every six hours for degree postings. To verify and augment these data, radiosondes were launched from near the Mauna Loa Observatory (on the northern flank of Mauna Loa, 10 km north of the validation site) when the satellites passed overhead. Profiles to longwave transmissivity, path radiance, and downwelling irradiance spectra were calculated using MODTRAN4[5]. These data were used to convert the measured radiance at sensor to land-emitted radiance, with the reflected downwelling irradiance removed in proportion to the reflectance measured in the laboratory.

Emissivities and surface temperatures were recovered from the land-emitted radiance, using the temperature-emissivity separation (TES) algorithm[1] for ASTER and using the model emissivity approach[6] for MTI Band N (~10.5μm). The model emissivity calculation requires that the emissivity at one wavelength be known independently. Ground measurements satisfy this requirement. We used an emissivity of 0.96 (based on ground samples) to calculate the kinetic temperature for MTI band M, and then used this temperature to calculate the model emissivity for MTI band N.

2.2.2 **Analysis of field data**

One dimensional semivariograms were computed for observed brightness temperatures and retrieved emissivity for sub-images containing the study area for both sensor systems. Semivariograms describe the relationship of one point to others over varying distances and thus describe the scales at which pixels are related to each other. In addition, semivariograms were calculated for both the temporal and spatial varying ground based radiometer measurements. A semivariogram was also calculated for the laboratory measurements of ground samples. The semivariograms are the basis for comparison of the scale of variance for the different data sets.

3. RESULTS & DISCUSSION

Figure 2a shows the retrieved emissivity image for MTI band N for the study area and immediate surroundings. It is distinct from surrounding basalt and quite uniform. Figure 2b shows the image of retrieved emssivity for the same area. (There is a very strong contrast stretch applied to the emissivity image in Figure 2b.) The one dimensional semivariogram taken near the data transect, given in Figure 3, shows little spatial structure. The plot is for 5 rows of data in the intensive study area averaged together. The weak shape of the curve, with its peak at 140 m, is thought to be artifact as there was a great deal of variability between the individual rows. Even if real, the magnitude is very small. The same holds true for semivariograms made for the ASTER image, not shown here. The semivariogram for the ground emissivity measurements shown in Figure 4 again shows no spatial coherence. They are small area samples and therefore show greater variability than the image data. Figure 5 shows the time series of radiometer measurements made "walking around" and shows variations commonly about 10C on July 15. These measurements are separated by about 1 m in the densest portion of the data and these variations would be reduced by spatial averaging in a remote sensing system: the standard deviation of MTI retrieved temperatures is less than 1C. A semivariogram was made

from ground based radiometer measurements and is shown in Figure 6. The data for this calculation was taken from one straight, uniform "walk" with 61 measurements made at 1 sec. intervals made very close to 1 m apart. Even at this spatial resolution, about 1m, little spatial coherence is seen except, perhaps, in the 1 – 3 m scale. We feel that spatial

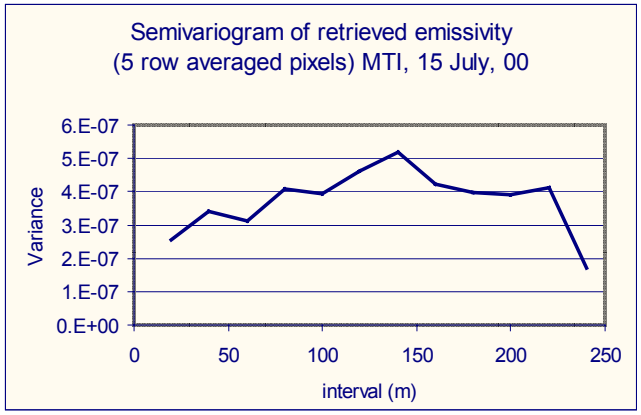

Figure 3. Semivariogram of retrieved emissivity, MTI band N.

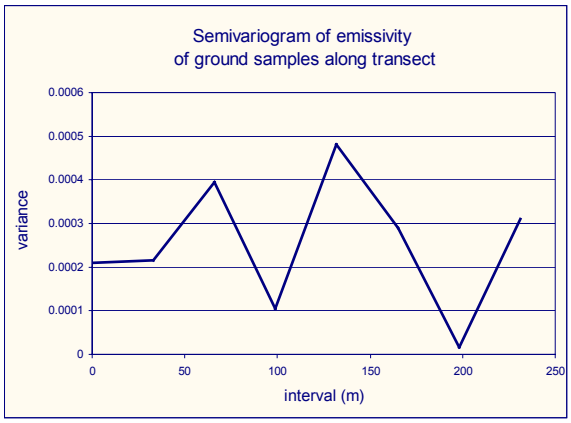

Figure 4. Semivariogram of ground sample emissivity.

structure at this scale is due to regular patterns of the cooling polygons and the cracks between them. Note also that these measurements were obtained over a period greater than 20 minutes, and while there is no temporal trend in the July 15 data, there are significant temporal fluctuations . Radiometer data taken at one location over time shows that 5C variation of temperature of a small spot was common: these purely temporal fluctuations approach half the magnitude of the variation observed 'walking around'. (In the late morning on the day before, temporal and spatial fluctuations were similar.) The time series at the stationary point on 15 July is shown in Figure 7. A power spectrum done on a subset of data showed a peak at six minutes. On the day before (14^{th}), a peak was seen at 5 minutes. While there is likely to be variability of the structure of the temporal fluctuations, they always seem to be on the scale of a few minutes. Since the 'walking around' data contain both spatial and temporal variation, the temporal data indicate that on this day, the temporal variations approach the same magnitude as the spatial variation, as measured from the ground.

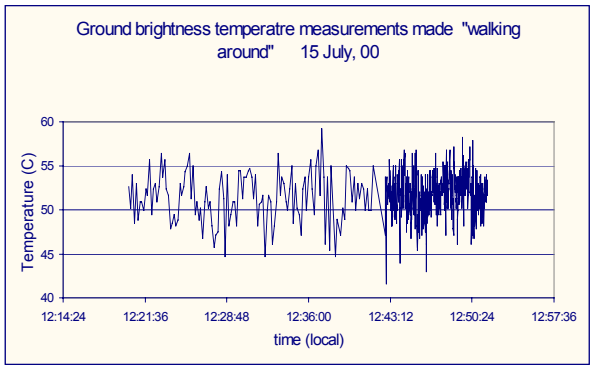

Figure 5. Ground based brightness temperature measurements made 'walking around' the FOV of the camera on the rim.

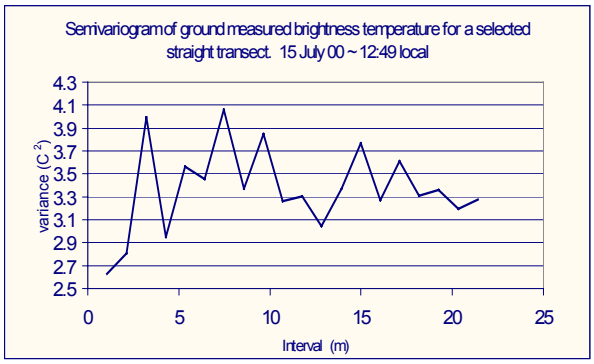

Figure 6. Semivariogram of a 6 minite segment of data shown in Figure 5 centered at 12:49 local time.

The impact of temporal variations on the spatial variation of surface temperature is graphically and dramatically seen in imagery taken from the caldera rim on July 14 by Dr. Lance O'Steen Figure 8 shows a false color composite of three images taken at roughly 3 minutes apart. The different colors denote different hot regions at different times. Note that while spatial structure is obvious in the scene, it is at fine scale.

The analyses we performed with one dimensional spatial statistics showed no spatial structure of emissivity of the surface. The emissivity of ground samples also show no spatial coherence in the intensive study area. Also, a 'spatial' sample transect of radiometric temperature measurements made in a short period of time also showed no spatial structure except perhaps at very small scales. Temporal structure of temperature, however, was clear, if variable, and of a large magnitude.

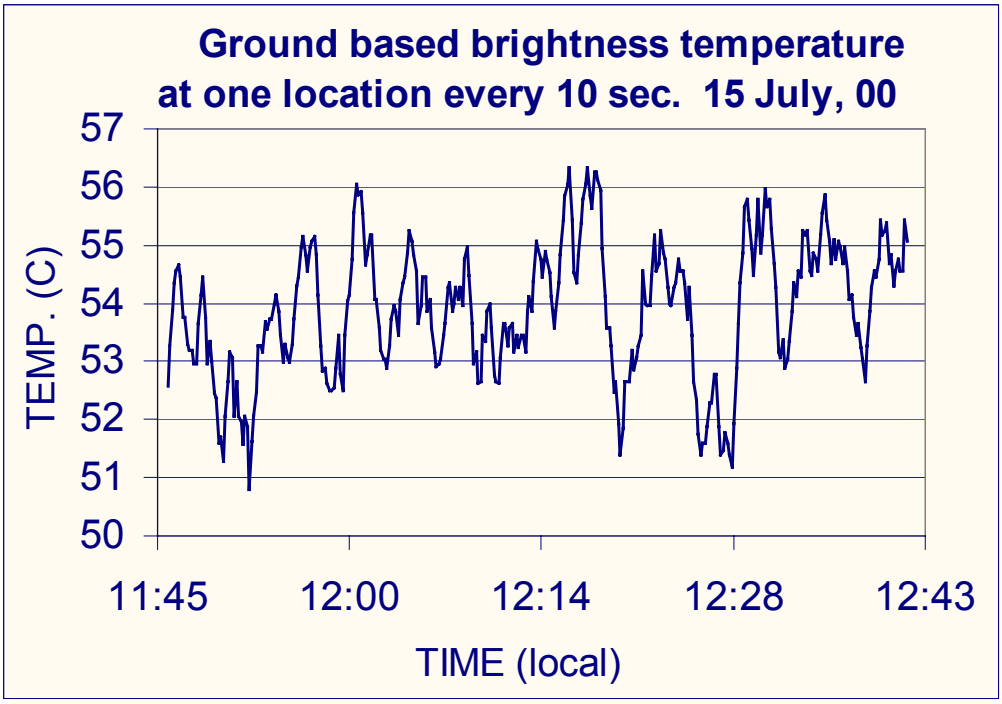

Figure 7. Time series of brightness temperature measured with a ground based radiometer a single location every 10 seconds.

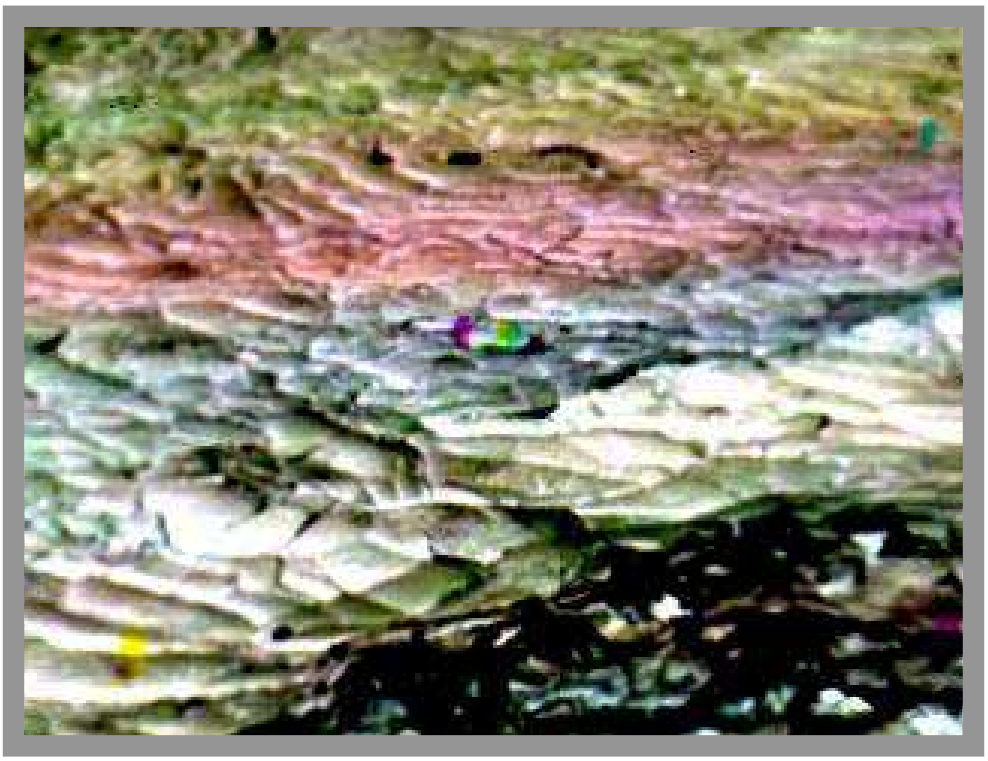

Figure 8. False color composite image for three frames from a thermal IR camera on the caldera rim on 14 July, 00. The composite is made from images at 11:32 (red), 11:30 (green) and 11:27 (blue) local time and the colors indicate movement of warm/cold spatial distribution on the scale of minutes.

4. CONCLUSIONS

The spatial variance of emissivity in the intensive study area is at spatial scales beneath those resolvable by ASTER or MTI. 1-D semivariograms of the satellite (ASTER, MTI) data show little if any spatial coherence. The lack of coherence means that classical random sampling of ground samples is appropriate. Patterns of temperature related to the surface are observed by ground based imaging due to the cooling polygons, and spatial coherence is on the order of 1 - 3 m. This is a very desirable feature of the intensive study site.

Transient temporal variation is roughly as important as spatial variations for satellites on uniform surfaces. These temporal variations (spot) are on the order of 5C on both 14 & 15 July '00, and these variations fluctuate on the scale of minutes. Since satellites make nearly instantaneous measurements, transient temporal variations must be taken into account. The practical way to do this is to average spatially at a scale where the transient fluctuations are smoothed. Spatial averaging of the MTI images suggest that the minimum area needed to be averaged is roughly 100m x 100m, about the size of an ASTER pixel. MTI pixels would need to be averaged in about 5 x 5 pixel dimensions to achieve a stable temperature measurement.

Trade-offs between spatial and temporal averaging need to be better understood and be evaluated in quantitative terms directly useful to remote sensing issues. The complexity of these tradeoffs will be large.

It may be necessary to use airborne thermal IR imagery for satellite vicarious thermal validation in order to cover the calibration site in a short time at view angles similar to the satellite. Airborne data (TIMS, MASTER) will be used in the future to better examine spatial variance at scales between the ground measurements and the satellite data.

Future work will emphasize small spatial scales utilizing airborne scanner imagery, both old and new. We were largely unable to address the general issues related to scaling in this paper due to the emphasis placed on the intensive study area and the temporal issues which are apparent on a background of quite uniform emissivity rock. Investigations over larger, less controlled areas are envisioned once the temporal variations in the intensive study area are sufficiently well characterized.

ACKNOWLEDGEMENTS

This work was supported, in part, by the Multispectral Thermal Imager Project of the Department of Energy through contract W-7405-ENG-36 with the University of California. We would also like to acknowledge the Savanna River Technology Center MTI ground measurement team for their comprehensive collection of ground data.

REFERENCES

1. R., Matsunaga, T., Rokugawa, S., and Hook, S. J., "Temperature and Emissivity Separation from Advanced Spaceborne Thermal Emission and Reflection Radiometer (ASTER) Images" *IEEE Transactions on Geoscience and Remote Sensing*, **36**, 1113-1126. 1998.
2. Price, J. C., "Land surface temperature measurements from the split window channels of the NOAA-7 advanced very high resolution radiometer", *Jour. Geophys. Research* **89**, 7231-7237. 1984.
3. Gu, D., Gillespie, A. R., Kahle, A. B., and Palluconi, F. D., "Autonomous atmospheric compensation (AAC) of high resolution hyperspectral thermal infrared remote-sensing imagery*", IEEE Transactions on Geoscience and Remote Sensing*, **38**(6), 2557-2570. 2000.
4. Palluconi, F. D., and Meeks, G. R., "Thermal Infrared Multispectral Scanner (TIMS): An Investigator's guide to TIMS data", JPL Publication 85-32. 1985.
5. Kniezys, F. X., Abreu, L. W., Anderson, G. P., Chetwynd, J. H., Shettle, E. P., Berk, A., Bernstein, L. S., Robertson, D. C., Acharya, P., Rothman, L. S., Selby, J. E. A., Gallery, W. O., and Clough, S. A., 1996. The MODTRAN 2/3 report and LOWTRAN 7 model. Edited by L. W. Abreu and G. P. Anderson, Phillips Lab., Geophys. Directorate, PL/GPOS, Hanscom AFB, MA 01731, Contract F19628-91-C-0132, 1 November.
6. Gillespie, A. R., Kahle, A. B., and Walker, R. E., "Color enhancement of highly correlated images, I. Decorrelation and HSI contrast stretches. *Remote Sens. Environ.* **20**, 209-235. 1986.